# Automated Laser Ablation of Motile Sperm for Immobilization

Zhuoran Zhang, Changsheng Dai, Xian Wang, Changhai Ru, Khaled Abdalla, Sahar Jahangiri, Clifford Librach, Keith Jarvi, and Yu Sun

***Abstract*—Automated manipulation of single cells is required in both biological and clinical applications. In clinical infertility treatments, a single motile sperm is immobilized and inserted into an egg cell for in vitro fertilization. Sperm immobilization is essential to ease the ensuing pick-up procedure, and importantly, it prevents the sperm tail from beating inside the egg cell, which causes a lower fertilization rate. For immobilizing a motile sperm, the sperm tail must be accurately positioned and aligned with the manipulation tool (e.g., laser spot). Manual immobilization using laser ablation has stringent skill requirements, and is not able to accurately position the sperm tail to the center of the laser spot for immobilization. This paper presents a visual servo system that is capable of accurately positioning the tail of a motile sperm relative to the laser spot for automated sperm immobilization. A visual servo control strategy was developed to estimate and compensate for the motion of the sperm tail. Experimental results showed that the visual servo controller achieved a positioning accuracy of 1.7 $\mu$m, independent of sperm speed or swimming direction. By quantitatively evaluating the effect of laser energy on sperm immobilization, a consistent immobilization success rate of 100% was achieved (based on experiments on 900 sperms) with a throughput five times that of manual operation. Experimental results confirmed that this automated immobilization technique did not induce damage to sperm DNA.**

***Index Terms*—Automation at Micro-Nano Scales, Biological Cell Manipulation**

## I. INTRODUCTION

LASER ablation has been widely used in manufacturing, material synthesis, and precision surgery. In life sciences, laser ablation is used for precisely cutting/separating various structures in tissues, cells, and molecules. Laser ablation requires the laser spot to be precisely aligned with the ablation target. While most targets are immobile, accurately positioning a motile target (a swimming sperm, moving molecules [1], and motor proteins [2]) relative to the laser spot is challenging. This work aimed to realize automated laser ablation of the molecular motors in a motile sperm tail for immobilization, without causing DNA (deoxyribonucleic acid) damage to the sperm. Sperm immobilization is an essential step in clinical infertility treatment. In clinical practice, after a sperm is immobilized, the sperm is picked up using a glass micropipette then inserted into the egg cell to achieve in vitro fertilization (IVF) [3].

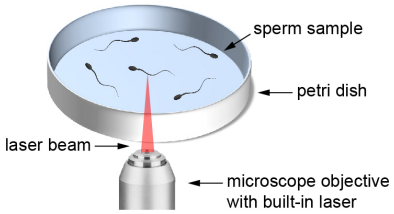


Fig. 1. Schematic illustration of laser ablation for sperm immobilization. The sperm tail is aligned with the laser spot and laser pulses are fired to ablate the molecular motors. The sperm tail must be accurately positioned in the laser spot for effective sperm immobilization and to avoid damaging DNA that resides in the sperm head.

The conventional sperm immobilization method uses a glass micropipette to tap the sperm tail against a substrate [4], [5]. This method is limited to immobilizing sperms that swim in a direction aligned nearly perpendicular to the micropipette axis. A sperm whose tail axis is in parallel with the micropipette axis cannot be immobilized because the sperm head would be unavoidably tapped by the micropipette and damaged. The orientation of such sperms must be adjusted (e.g., using a rotational microscopy stage [6]) before sperm immobilization is performed.

An alternative method for sperm immobilization is to use laser pulses to ablate the motor proteins in the sperm tail (see Fig. 1). Compared with the conventional micropipette tapping method, this non-contact approach is suitable for immobilizing a sperm that swims in an arbitrary direction. In manual laser-based sperm immobilization [7], [8], a trained embryologist looks through the microscope eyepieces and dexterously moves the microscope stage to position the sperm tail towards and into the laser spot. Due to the fast movement of motile sperms (>25 $\mu$m/s) and the tail's beating movement (5-10 Hz) [9], this accurate positioning task is challenging for human operators. In practice, a human operator makes several attempts to aim at the sperm tail and repeats the

Manuscript received: September 10, 2018; Revised November 26, 2018; Accepted December 20, 2018. This paper was recommended for publication by Editor Eric Marchand upon evaluation of the Associate Editor and Reviewers' comments. This work was supported in part by the Natural Sciences and Engineering Research Council of Canada through a Discovery Grant, the Canada Research Chairs Program, and in part by the University of Toronto via a Connaught Innovation Award. C. Ru acknowledges financial support from the National Natural Science Foundation of China (Grant No. 61774107).

Z. Zhang, C. Dai, X. Wang, and Y. Sun are with Department of Mechanical and Industrial Engineering, University of Toronto, 5 Kings College Road, Toronto, ON M5S 3G8, Canada. Correspondence to sun@mie.utoronto.ca

C. Ru is with Research Center of Robotics and Micro System & Collaborative Innovation Center of Suzhou NanoScience and Technology, Soochow University, Suzhou 215021, China.

K. Abdalla, S. Jahangiri, and C. Librach are with CReATe Fertility Centre, 790 Bay Street, Toronto, ON M5S 1N8, Canada.

K. Jarvi is with Mount Sinai Hospital, 600 University Avenue, Toronto, ON M5G 1X5, Canada.

Digital Object Identifier (DOI): see top of this page.

firing of laser pulses before sperm immobilization is achieved, making the process tedious and time-consuming (∼15 seconds per sperm) [7] with varying success rates across operators. Furthermore, poor position control based on trial and error in manual immobilization has a risk of mistakenly firing laser pulses close to or on the sperm head, causing damages to DNA. To realize automated sperm immobilization, techniques must be developed for accurately positioning the sperm tail relative to the laser spot.

Visual servo approaches have been developed for positioning objects under microscopy imaging, the majority of which focused on the visual servo of stationary objects such as micro parts [10] and immotile cells [11]. Methods have also been developed for accurate positioning of microswimmers. For instance, the dynamics of magnetic helical microswimmers was modeled, and both position-based [12] and image-based visual servo [13] have been implemented. However, these microswimmers are synthesized structures that do not have intrinsic movements. Thus, the positioning accuracy of these methods mainly depends on the accuracy of actuation. In contrast, a sperm is motile, constantly beating its tail and wiggling around its swimming path. For visual servo of cells with intrinsic movements, existing systems used fluid flow [14], electrical field [15] or laser trapping [16] for restricting a motile cell within a certain area without fine positioning accuracy requirements, whereas accurate positioning of a fast-moving cell to a specific target location has not been realized.

This paper reports an automated system capable of visually servoing the microscope stage (thus motile sperm) and automatically firing laser pulses for sperm immobilization with a high success rate and high throughput. A visual servo control strategy was developed to estimate and compensate for sperm motion for accurate position control. The system achieved a consistent immobilization success rate of 100% (n=900 sperms), with a throughput five times that of manual operation. Furthermore, experimental results confirmed that automated immobilization using laser ablation did not damage sperm DNA, promising safe and reliable clinical use.

## II. SYSTEM OVERVIEW

The system was built around a standard inverted microscope (Nikon Ti-S) which is equipped with an infrared laser (LYKOS, Hamilton Thorne Ltd.). The laser was built within a 40X microscope objective (see the inset of Fig. 2) and has a wavelength of 1.46 $\mu$m (infrared) and a maximum power of 300 mW. This infrared laser is commonly used in IVF clinics, such as for assisted embryo hatching and biopsy of preimplantation embryos. A camera (Basler acA1300-gc) and a motorized X-Y translational stage (Prior Scientific Inc.) were mounted on the microscope, forming a visual servo control system. Images were captured in 1200×900 pixels at 30 frames per second under bright-field imaging.

Sperm immobilization starts with the indication of a target sperm by a human operator via computer mouse clicking. This one-time user input allows the user or embryologist to practice their knowledge on sperm selection. Once a sperm is selected, the system begins to visually track the sperm tail to provide feedback for visual servo control. After the sperm tail is visually servoed to the laser spot, a laser pulse is triggered to immobilize the sperm.

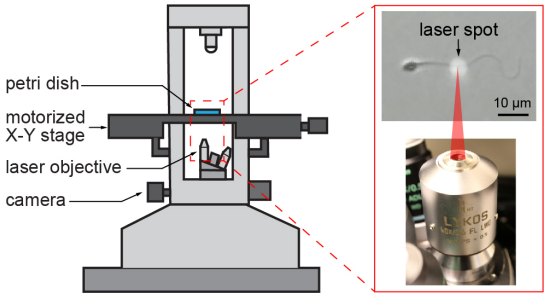


Fig. 2. The setup of the laser-based sperm immobilization system. The camera and motorized X-Y stage together form a 2-degree-of-freedom (DOF) eye-to-hand visual servoing system for automated sperm immobilization. The inset is the laser built within a 40X microscope objective. The laser spot size (i.e., the radius of the laser beam) is 2.6 $\mu$m.

## III. VISUAL SERVO CONTROL OF MOTILE SPERM

### A. Task Description

*1) Visual servoing scheme:* Since the laser was fixed in the microscope objective without a translational degree of freedom and only fired laser pulses at a fixed location in the X-Y plane, the motorized X-Y translational stage was controlled to position the sperm tail towards and in the laser spot. The Z position of the laser spot was not controlled because laser pulses were always focused in the same Z-plane as the imaging focal plane for focusing on sperm samples. In this visual servoing configuration, the position of the laser spot was fixed in the image frame, and the positions of the sperm tail were obtained from visual tracking. Hence, image-based visual servoing was performed.

*2) Positioning accuracy constraint:* The center of the laser spot has maximum intensity. The radial distance to the laser center, at which the laser intensity reaches $1/e^2$ of the maximum laser intensity, defines the size of the laser spot. The spot size of the 1.46 $\mu$m-wavelength laser used in this work is 2.6 $\mu$m [17]. The spot size is an intrinsic property of the laser and does not change with laser energy or power. After a laser pulse is fired, laser energy is transferred to the surrounding medium in the form of heat and causes temperature rise in the medium. Since the intensity of the laser used in this work follows a Gaussian distribution [17], temperature rise is the highest within the laser spot, for instance, ∼150°C at 2.6 $\mu$m to the laser center at 30 $\mu$J laser energy [18]. Through thermal conduction, heat is transferred to the medium outside the laser spot, and temperature rise rapidly decreases outside the laser spot (e.g., decreases to zero at 5.1 $\mu$m to the laser center at 30 $\mu$J laser energy [18]). Hence, the largest positioning error of visual servoing should be smaller than 2.6 $\mu$m to the laser center such that the sperm tail is positioned within the laser spot where the temperature is the highest.

*3) Laser energy selection:* Laser energy selection is a trade-off between sperm immobilization success rate and safety. On the one hand, the laser energy should be sufficiently high to ablate the sperm tail for immobilization. Higher laser energy causes temperature increase at a further distance to the laser

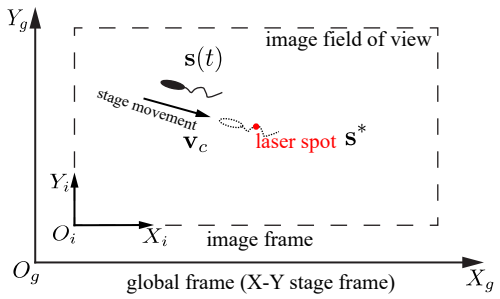


Fig. 3. Coordinate frames used in the visual servoing task. Velocity of the stage $\mathbf{v}_c$ is defined in the global frame. The sperm position $\mathbf{s}(t)$ at time instance $t$ and the target position of the laser spot $\mathbf{s}^*$ are defined in the image frame, forming imaging-based visual servo control.

center, thus offering more tolerance to the error in positioning the sperm tail. On the other hand, high laser energy has a risk of damaging the DNA in the sperm head because the temperature at the sperm head can be higher than 37°C. It is desired that only the sperm tail is ablated while the temperature at the sperm head remains at 37°C so that sperm DNA that is all in the sperm head is not affected.

### *B. Visual tracking of sperm tail*

To obtain visual feedback of sperm tail position, we used the tail tracking method in [6], [19] because of its robustness and high accuracy. Briefly, the head position is first tracked, then the tail position is estimated based on the head position. The sperm head is segmented via adaptive thresholding, and positions of the sperm head in different image frames are tracked using a probabilistic data association filter. The sperm dynamics is modeled with the state variables containing the x-y position $[x_{head}, y_{head}]^T$ and the orientation $\theta$ of the sperm head. The head orientation $\theta$ is the angle between the sperm head major axis and the x axis. Adding $\theta$ into the state variables effectively distinguishes the target sperm from the non-target interfering sperms when sperms cross over each other.

The sperm tail position $[x_{tail}, y_{tail}]^T$ is estimated by extending the head major axis according to $\begin{bmatrix} x_{tail} \\ y_{tail} \end{bmatrix} = \begin{bmatrix} x_{head} \\ y_{head} \end{bmatrix} - \alpha \begin{bmatrix} \cos\theta \\ \sin\theta \end{bmatrix}$, where $\alpha$ is a scalar determining the spatial distance between the estimated tail position and the head position. In our experiments, $\alpha$ was set to be 10 $\mu$m from the sperm head position. This distance ensures that the obtained tail position is neither too close to the sperm head so laser firing would not damage the sperm head, nor too far from the sperm head such that the obtained tail position would not fluctuate too much due to tail beating.

### *C. Visual Servo Controller Design*

The purpose of visual servoing is to position the sperm tail inside the laser spot, i.e., to minimize the error $\mathbf{e}(t)$

$$\mathbf{e}(t) = \mathbf{s}(t) - \mathbf{s}^* \tag{1}$$

where $\mathbf{s}(t) = [x_{tail}, y_{tail}]^T$ is the obtained sperm tail position in the image frame $X_iO_iY_i$ (Fig. 3), and $\mathbf{s}^*$ is the position of the laser spot in the image frame, which is a constant.

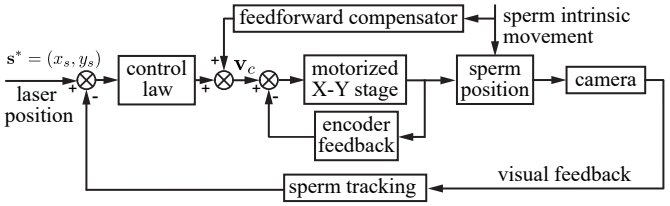


Fig. 4. System control diagram. A feedforward compensator is designed to compensate for sperm intrinsic movement. The target position $\mathbf{s}^* = (x_s, y_s)$ is the fixed position of the laser spot in the image field of view.

We first assume the sperm has no locomotion. Applying a velocity $\mathbf{v}_c$ to the motorized X-Y stage in the global frame changes the position of the sperm in the image frame. Changes in the sperm tail position $\mathbf{s}(t)$ are only caused by the motion of the stage, which gives

$$\dot{\mathbf{s}} = \mathbf{J}\mathbf{v}_c \tag{2}$$

where $\mathbf{J}$ is the image Jacobian matrix in the form of $\mathbf{J} = k\mathbf{I}_2$, where $\mathbf{I}_2$ is a 2×2 identity matrix, and $k$ is a constant given by $k = \text{focal length}/(\text{pixel size} \times \text{depth})$.

Combining (1) and (2) gives

$$\dot{\mathbf{e}} = \dot{\mathbf{s}} = \mathbf{J}\mathbf{v}_c \tag{3}$$

By assuming an exponential decoupled decrease of the error $\dot{\mathbf{e}} = -\lambda\mathbf{e}$, a proportional control law [20] is obtained

$$\mathbf{v}_c = -\lambda\mathbf{J}^{-1}\mathbf{e} \tag{4}$$

where $\lambda$ is the control gain.

The controller in (4) does not yet include the motion of the sperm. For a motile sperm, changes in the sperm tail position $\mathbf{s}(t)$ and the error $\mathbf{e}$ stems from not only the motion of the stage, but also the intrinsic movement of the sperm. Hence, (3) is modified according to [20] to

$$\dot{\mathbf{e}} = \dot{\mathbf{s}} = \mathbf{J}\mathbf{v}_c + \frac{\partial \mathbf{e}}{\partial t} \tag{5}$$

where $\frac{\partial \mathbf{e}}{\partial t} \neq 0$ represents the time variation of error $\mathbf{e}$ due to sperm motion. Substituting the control law (4) into (5) gives

$$\dot{\mathbf{e}} = -\lambda\mathbf{J}\mathbf{J}^{-1}\mathbf{e} + \frac{\partial \mathbf{e}}{\partial t} \tag{6}$$

and the error $\mathbf{e}$ does not converge to zero since $\frac{\partial \mathbf{e}}{\partial t} \neq 0$.

To ensure that the error converges to zero, the term $\frac{\partial \mathbf{e}}{\partial t}$ must be compensated by the controller. Hence, we designed a feedforward compensator to compensate for sperm motion (Fig. 4). The controller output $\mathbf{v}_c$ is accordingly changed to

$$\mathbf{v}_c = -\lambda\mathbf{J}^{-1}\mathbf{e} - \mathbf{J}^{-1}\widehat{\frac{\partial \mathbf{e}}{\partial t}} \tag{7}$$

where $-\mathbf{J}^{-1}\widehat{\frac{\partial \mathbf{e}}{\partial t}}$ is the output of the feedforward compensator, and $\widehat{\frac{\partial \mathbf{e}}{\partial t}}$ is the estimated velocity of the sperm [20].

To estimate $\widehat{\frac{\partial \mathbf{e}}{\partial t}}$, in experiments, the X-Y stage was turned off for 30 image frames (1 second) so that the measured $\dot{\mathbf{e}}$ was only caused by sperm movement. Considering that a sperm wiggles around its swimming path and may exhibit abrupt

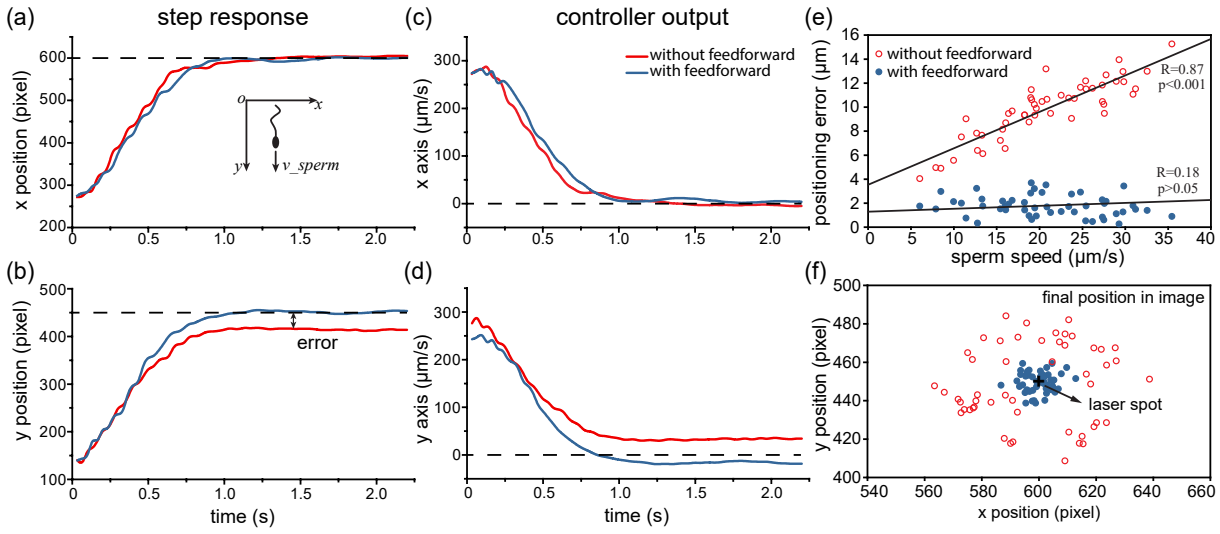


Fig. 5. Performance of visual servoing. (a)-(d) Two controllers (with/without feedforward) were applied on the same sperm to compare their performance. The sperm was swimming along the y-axis with less than 1 $\mu$m/s velocity along the x-axis. (a)(b) The step response of the two controllers along (a) x-axis and (b) y-axis. The dashed line is the target position. (c)(d) Controller output of the two controllers along (c) x-axis and (d) y-axis. The dashed line indicates when the output reaches zero. (e) Without compensating for sperm motion, the positioning error significantly increase with sperm speed. A consistent positioning error is achieved after compensating for sperm motion by the feedforward controller. The solid line is the fitted trend line (n=50 sperms for each line). R: correlation coefficient. p: p-value calculated by t-test trend analysis. (f) Final position of each sperm after visual servoing. The sperm positions with feedforward are less spread than those without feedforward, yielding better positioning accuracy by the feedforward controller.

changes in its movement direction and/or velocity between two successive image frames, the average velocity over the 30 image frames was calculated

$$\widehat{\frac{\partial \mathbf{e}}{\partial t}} = \frac{1}{30}\sum_{k=0}^{29}[\mathbf{s}(t-k)-\mathbf{s}(t-k-1)] \tag{8}$$

The feedforward compensator ensures that the error $\mathbf{e}$ converges to zero. Substituting (7) into (5) gives

$$\dot{\mathbf{e}} = -\lambda \mathbf{J}\mathbf{J}^{-1}\mathbf{e} - \mathbf{J}\mathbf{J}^{-1}\widehat{\frac{\partial \mathbf{e}}{\partial t}} + \frac{\partial \mathbf{e}}{\partial t} \tag{9}$$

and the error converges to zero as long as $\widehat{\frac{\partial \mathbf{e}}{\partial t}} = \frac{\partial \mathbf{e}}{\partial t}$, i.e., the estimated sperm motion (velocity) is sufficiently close to the real sperm motion. After the sperm reaches the target position, a laser pulse is automatically fired by the system to ablate the motor proteins in the sperm tail for immobilizing the sperm.

## IV. EXPERIMENTAL RESULTS AND DISCUSSION

Human sperm samples were obtained from CReATe Fertility Centre in Toronto. The study protocol was approved by the University of Toronto Research Ethics Board, and informed consent was obtained from all subjects. As in clinical practice, sperm samples were placed in the sperm wash medium (Irvine) mixed with 7% polyvinylpyrrolidone (PVP). In all experiments the medium was covered by mineral oil to prevent evaporation.

### A. Performance of visual servoing and system throughput

Two controllers were applied to visually servo the same sperm to evaluate and compare their control performance. In the first controller, the feedforward compensator was intentionally disabled, and the controller followed (4). The second controller was implemented as shown in the control diagram in Fig. 4 where the feedforward compensator was turned on and the controller output followed (7). A sperm swimming along the y-axis with a low velocity ($<$1 $\mu$m/s) along the x-axis was intentionally chosen for comparing the performance of the two controllers. The sperm tail visual tracker, as previously reported in [6], has a success rate of $>$96.0% with a tail tracking accuracy of 1.08 $\mu$m.

As summarized in Fig. 5(a)(c), both controllers brought the sperm to the target position in the x-axis along which the sperm was largely motionless. Both the error and controller output converged to zero. For the y-axis along which the sperm was swimming, the first controller without feedforward failed to bring the sperm to the target position [see red curve in Fig. 5(b)]. As revealed and explained by Eq. (6), the error did converge, but to a non-zero value. The converged controller output (i.e., velocity of the stage) was equal to the sperm's velocity along the y-axis [converged controller output: $\sim$35 $\mu$m/s, see red curve in Fig. 5(d)]. Hence, the converged controller output was cancelled out by the sperm's motion, without further reducing the positioning error. In contrast, the second controller with feedforward successfully positioned the sperm to the target position [Fig. 5(b)(d)], confirming the effectiveness and necessity of estimating and and compensating for sperm motion, according to (7) and (8).

Visual servoing was repeated on 100 randomly chosen sperms (50 sperms by each controller). Without compensating for sperm motion, the positioning error significantly increased with sperm's swimming speed ($p<0.001$ by t-test trend analysis), and the spread of sperm positions after visual servoing was wide [see Fig. 5(e)(f)]. The dependency of the positioning error on sperm speed can be explained by analyzing (6), where the uncompensated term $\frac{\partial \mathbf{e}}{\partial t}$ remains in the solution of the

error **e**. For positioning a sperm with a speed of 35 $\mu$m/s, the positioning error can be as large as 15 $\mu$m, which is approximately 30% of the length of a sperm tail, and laser firing would miss the sperm tail and cause immobilization failure. In contrast, the positioning error of the feedforward controller was consistent and did not increase with sperm speed ($p>0.05$). The average positioning error of the feedforward controller was significantly smaller than that without feedforward ($1.7\pm0.8$ $\mu$m vs. $9.8\pm2.4$ $\mu$m, $p<0.001$). The average positioning error of 1.7 $\mu$m is smaller than the laser spot size (2.6 $\mu$m), thus ensuring that firing laser pulses would not miss the sperm tail. Overall, the designed feedforward compensator significantly improved the positioning accuracy for sperm immobilization.

In terms of throughput, the system completed automated sperm immobilization within 3 seconds (1 second for sperm locomotive measurement; 1-2 seconds for visual servoing, depending on the sperm's original position). In contrast, manual operation by experienced embryologists using laser ablation costs approximately 15 seconds per sperm [7]. Automated immobilization yields a throughput five times that of manual operation. This is because a human operator lacks the capability of accurately positioning the fast-beating sperm tail and firing laser pulses would miss the sperm tail. In the case of failure, the human operator repeats aiming at the sperm tail, positioning the sperm tail by trial and error, and firing laser pulses until the sperm is immobilized. With accurate visual servoing, our automated system is capable of immobilizing a target sperm with only one shot (laser pulse).

### *B. Immobilization success rate*

An immobilization process was considered successful when a target sperm was permanently immobilized with no observable locomotion of its tail after immobilization. Since the performance of immobilization is determined by the energy delivered by the laser to the sperm tail, we evaluated the effect of laser energy on immobilization success rate. By adjusting laser pulse duration (in $\mu$s), we experimentally tested six laser energy levels (Fig. 6). At each energy level, 150 sperms (in 3 independent experiments and 50 sperms in each experiment) were immobilized by the system, and their respective success rates were quantified. All sperms were randomly chosen with random swimming directions and speeds.

It was found that at a low laser energy of 3 $\mu$J, although the laser spot was aligned with the sperm tail, firing laser pulses did not affect sperm locomotion at all. After firing laser pulses, the sperms did not even show decrease in swimming speed. At a higher laser energy level between 6 $\mu$J and 12 $\mu$J, an increasing percentage of the sperms was successfully immobilized (Fig. 6). In the failure cases, the sperms either slightly slowed down their swimming speed or were temporarily immobilized but recovered their locomotion (typically within a minute) after laser firing. This might be due to the mechanism of laser ablation that relies on the increase in local temperature within and around the laser spot. At a relatively low laser energy level, the temperature increase was not sufficient to affect the molecular motors on the sperm tail, resulting in partial but not complete ablation of the molecular motors.

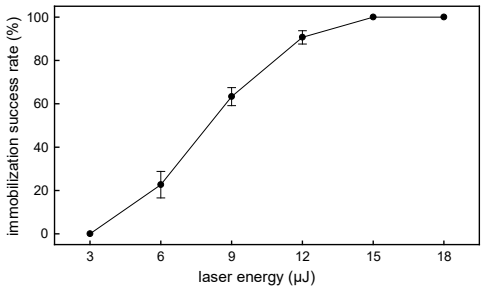


Fig. 6. Immobilization success rate increased with laser energy. A consistent success rate of 100% was achieved with laser energy above 15 $\mu$J. Error bar represents standard deviation from three independent experiments, and in each experiment 50 sperms (900 sperms in total) were immobilized to quantify success rate.

A consistent success rate of 100% was achieved at the laser energy higher than or equal to 15 $\mu$J (Fig. 6). As discussed in Section III.A.3), further increasing the laser energy has a higher risk of damaging the sperm head, where DNA resides, because the laser-induced temperature can be higher than 37°C in the sperm head region. Hence, laser energy was set to 15 $\mu$J (i.e., 50 $\mu$s pulse length at 300 mW power) in our system to avoid potential damage to sperm DNA while achieving 100% success rate in sperm immobilization.

### *C. Immobilization caused no sperm DNA damage*

To evaluate the safety of the automated sperm immobilization technique, we measured sperm DNA integrity after sperm immobilization by laser ablation to investigate whether laser-based immobilization causes damage to sperm DNA. Since DNA measurement is an invasive process requiring the sperm to be lysed and it is infeasible to compare the DNA status of the same sperm before and after immobilization, we measured and compared DNA integrity on sperm populations. We randomly chose 100 sperms and split them into two groups: the control group where 50 sperms were not immobilized and the experimental group where 50 sperms were immobilized by the automated laser-ablation system.

Sperm DNA damage was measured by the single-cell gel electrophoresis method (i.e., the Comet assay). This method was chosen because it is the only method capable of quantitatively measuring the extent of DNA damage in a single sperm [21]. Briefly, a sperm is deposited into the agarose gel, then sperm membrane and chromatin proteins are lysed to expose DNA strands. Electrophoresis is then performed to allow DNA fragments, which are negatively charged, to migrate within the agarose gel and form the comet shape under fluorescent imaging [see Fig. 7(a)]. Intact DNA strands do not migrate and remain in their original position, forming the comet head [see Fig. 7(a)]. DNA damage were measured by two commonly used metrics: percentage of DNA in the comet tail (i.e., percent of damaged DNA) and comet tail moment (i.e., percent of damaged DNA$\times$the maximum migration distance) [22]. For each group, the three lines of the box represent 75 percentile, median, and 25 percentile [Fig. 7(b)(c)]. The two groups had the same data distribution, and no significant difference was found in terms of both percent DNA in comet tail [Fig. 7(b)] and comet tail moment [Fig. 7(c)]. The results

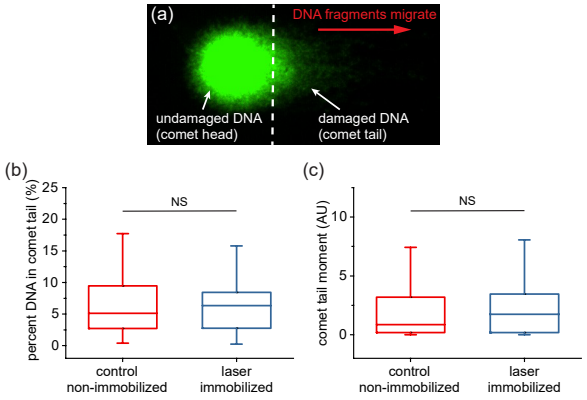


Fig. 7. Automated laser-based immobilization induced no damage to sperm DNA. (a) DNA damage was measured by single-cell gel electrophoresis (Comet assay). Damaged DNA fragments are negatively charged and migrate during electrophoresis, thus forming a comet tail. (b)-(c) No significant difference was found in (b) percentage of DNA in the comet tail and (c) comet tail moment between immobilized sperms (n=50) and non-immobilized sperms (n=50). AU: arbitrary unit. NS: not statistically significant.

indicate that automated laser-based immobilization caused no significant damage to sperm DNA and confirmed its safety for clinical use.

The fact that laser ablation caused no significant DNA damage can be attributed to the system's accurate positioning capability and the sufficiently but not too high laser energy used. The thermal effects of the same 1.46 $\mu$m-wavelength laser used in our work were investigated in literature [18]. Under the laser energy of 30 $\mu$J, firing a single laser pulse caused a temporary temperature increase in the culture medium to as far as $\sim$5.1 $\mu$m from the laser center [18]. Beyond this distance, the temperature in the medium remains at 37°C without increase. Compared to [18], our system used only half the laser energy (15 $\mu$J vs. 30 $\mu$J). Furthermore, the medium used for sperm immobilization in our work contains the standard clinical material, polyvinylpyrrolidone (PVP) which has a lower thermal conductivity than the culture medium (0.45 $\mathrm{Wm^{-1}K^{-1}}$ vs. 0.60 $\mathrm{Wm^{-1}K^{-1}}$ [23]). Thus, the laser-induced temperature increase in our system is even more localized and restricted to a distance shorter than 5.1 $\mu$m to the center of the laser spot. Since the system accurately positioned the sperm tail to the laser spot, with the sperm head 10 $\mu$m away from the laser center, the temperature at the sperm head was kept at 37°C, thus resulting in no damage to DNA in the sperm head.

## V. CONCLUSION

This paper reported an automated system for laser-based sperm immobilization. Integrated with a visual servo controller which estimated and compensated for sperm locomotion, the system was capable of accurately positioning the tail of a motile sperm to the laser spot with an accuracy of 1.7 $\mu$m, independent of sperm speed and swimming direction. By quantitatively testing different laser energy levels, the system achieved a consistent 100% success rate for sperm immobilization. Automated sperm immobilization was completed within 3 seconds, which is four times faster than manual operation. DNA measurement results confirmed that this automated sperm immobilization technique did not induce extra damage to sperm DNA, confirming its safety for clinical use. The current one-second evaluation of single sperm locomotion is useful for measuring motility parameters of multiple sperms, permitting the selection of a target sperm with normal locomotion behaviors. This robotic sperm immobilization technique will be integrated with other cell manipulation techniques such as robotic sperm aspiration and robotic microinjection for robotic cell surgery in in vitro fertilization.

## REFERENCES

[1] T. Zhao et al., "Growing microtubules push the oocyte nucleus to polarize the Drosophila dorsal-ventral axis," *Science*, vol. 336, no. 6084, pp. 999–1003, 2012.
[2] R. Gonzalez et al., "Myosin II Dynamics Are Regulated by Tension in Intercalating Cells," *Dev. Cell*, vol. 17, no. 5, pp. 736–743, 2009.
[3] Z. Lu et al., "Robotic ICSI (Intracytoplasmic Sperm Injection)," *IEEE Trans. Biomed. Eng.*, vol. 58, no. 7, pp. 2102–2108, 2011.
[4] A. Velaers et al., "Triple touch sperm immobilization vs. single touch sperm immobilization in ICSI - a randomised trial," *Reprod. Biol. Endocrinol.*, vol. 10, no. 1, p. 1, 2012.
[5] C. Leung et al., "Automated sperm immobilization for ICSI," *IEEE Trans. Biomed. Eng.*, vol. 58, no. 4, pp. 935–942, 2011.
[6] Z. Zhang et al., "Robotic Immobilization of Motile Sperm for Clinical Intracytoplasmic Sperm Injection," *IEEE Trans. Biomed. Eng.*, vol. PP, no. 99, p. 1, 2018.
[7] T. Ebner, "Laser assisted immobilization of spermatozoa prior to intracytoplasmic sperm injection in humans," *Hum. Reprod.*, vol. 16, no. 12, pp. 2628–2631, 2001.
[8] M. Montag et al., "Laser-induced immobilization and plasma membrane permeabilization in human spermatozoa." *Hum. Reprod.*, vol. 15, no. 4, pp. 846–852, 2000.
[9] E. A. Gaffney et al., "Mammalian Sperm Motility: Observation and Theory," *Annu. Rev. Fluid Mech.*, vol. 43, no. 1, pp. 501–528, 2011.
[10] B. Tamadazte et al., "Robotic micromanipulation and microassembly using monoview and multiscale visual servoing," *IEEE/ASME Trans. Mechatron.*, vol. 16, no. 2, pp. 277–287, 2011.
[11] X. Liu et al., "Orientation control of biological cells under inverted microscopy," *IEEE/ASME Trans. Mechatron.*, vol. 16, no. 5, pp. 918–924, 2011.
[12] T. Xu et al., "Planar path following of 3-D steering scaled-up helical microswimmers," *IEEE Trans. Rob.*, vol. 31, no. 1, pp. 117–127, 2015.
[13] Y. Guan et al., "Image-based visual servoing of helical microswimmers for arbitrary planar path following at low reynolds numbers," *IEEE IROS*, pp. 1883–1888, 2017.
[14] Z. Zhang et al., "Human sperm rheotaxis: a passive physical process," *Sci. Rep.*, vol. 6, p. 23553, 2016.
[15] N. Ogawa et al., "Microrobotic Visual Control of Motile Cells Using High-Speed Tracking System," *IEEE Trans. Robot.*, vol. 21, no. 4, pp. 704–712, 2005.
[16] J. M. Nascimento et al., "The use of optical tweezers to study sperm competition and motility in primates." *J. Royal Soc. Interface*, vol. 5, no. 20, pp. 297–302, 2008.
[17] D. H. Hamilton et al., "Thermal effects in laser-assisted pre-embryo zona drilling." *J. Biomed. Opt.*, vol. 6, no. 2, pp. 205–213, 2001.
[18] C. Y. Wong and J. K. Mills, "Automation and optimization of multipulse laser zona drilling of mouse embryos during embryo biopsy," *IEEE Trans. Biomed. Eng.*, vol. 64, no. 3, pp. 629–636, 2017.
[19] J. Liu et al., "Quantitative Analysis of Locomotive Behavior of Human Sperm Head and Tail," *IEEE Trans. Biomed. Eng.*, vol. 60, no. 2, pp. 390–396, 2013.
[20] F. Chaumette et al., "Visual servo control. II. Advanced approaches," *IEEE Robot. Autom. Mag.*, vol. 14, no. 1, pp. 109–118, 2007.
[21] M. B. Shamsi et al., "Sperm DNA integrity assays: Diagnostic and prognostic challenges and implications in management of infertility," *J. Assist. Reprod. Genet.*, vol. 28, no. 11, pp. 1073–1085, 2011.
[22] P. L. Olive et al., "The comet assay: a method to measure DNA damage in individual cells." *Nat. Protoc.*, vol. 1, no. 1, pp. 23–29, 2006.
[23] M. Zhou et al., "Analysis of factors influencing thermal conductivity and viscosity in different kinds of surfactant solutions," *Exp. Therm Fluid Sci.*, vol. 36, pp. 22–29, 2012.